Journal of Magnetics 11(1), 43-50 (2006)

AFM Study and Magnetic Properties of Nanocrystalline $Fe_{73.5-x}Cr_xSi_{13.5}B_9Nb_3Au_1$ (x = 1~5) Alloys

Anh-Tuan Le[1], Nguyen Chau[2], Nguyen Duy Cuong[1], Ngo Duc The[2], Chong-Oh Kim[1], Jang-Roh Rhee[3], and Heebok Lee[4]*

[1]*Department of Materials Engineering, Chungnam National University, Daejeon 305-764, Korea*
[2]*Center for Materials Science, National University of Hanoi, 334 Nguyen Trai, Hanoi, Vietnam*
[3]*Department of Physics, Sookmyung Women's University, Seoul 140-742, Korea*
[4]*Department of Physics Education, Kongju National University, Kongju 314-701, Korea*

(Received 14 November 2005)

In this paper, the influences of microstructural and surface morphological developments on the soft magnetic properties and giant magneto-impedance (GMI) effect of the $Fe_{73.5-x}Cr_xSi_{13.5}B_9Nb_3Au_1$ (x = 1, 2, 3, 4, 5) alloys have been presented. It was found that the Cr addition slightly decreased the mean grain size of α-Fe(Si) grains. AFM results indicate a large variation of surface morphology of density and size of protrusions along the ribbon plane due to microstructural changes caused by thermal annealing with increasing Cr content. Ultrasoft magnetic properties of the nanocrystallized samples were noticeably enhanced by properly heat treatments at T_a=540°C such as an increase of the magnetic permeability and the decrease of coercivity, which is likely due to the formation of nanoscale α-Fe(Si) phase which reduced the magnetoelastic anisotropy of samples. Accordingly, the GMI effect was observed in the annealed samples. The correlation between the microstructure, surface morphology, and soft magnetic properties were explained by nucleation and growth model.

Key words : AFM, surface topography, microstructure, magnetic properties, nanocrystalline alloys

1. Introduction

Recently, the nanocrystalline soft magnetic alloy has attracted much research interest due to their fundamental scientific interest and their potential applications [1]. A special attention is paid on the nanocrystalline $Fe_{73.5}Si_{13.5}B_9Nb_3Cu_1$ alloy, commercially knows as FINEMET. The discovery of this alloy established a new approach to develop soft-magnetic materials with high magnetic flux density (B_s) that the magnetocrystalline anisotropy can be reduced by refining the grain size in less than a few tens of nanometers [2]. The optimum nanocrystallized state is obtained by isothermal annealing of the as-quenched amorphous ribbon above its dynamic crystallization temperature, typically in the range from 773 to 818 K for 1 hour [1-3]. After such a heat treatment the material shows a uniform structure of ultrafine crystallites (bcc FeSi) with average diameter of 10-20 nm embedded in the residual amorphous matrix. Structural changes, induced by annealing, modify the macroscopic magnetic behavior of the constituent material. Furthermore, the microstructure dependence of the magnetic properties was explained by the random anisotropy model, which is proposed for amorphous ferromagnets by Alben *et al.* [4] and developed by Herzer *et al.* [5]. According to this model, when the grain size is less than the ferromagnetic exchange length (L_{ex}), the exchange interaction dominates the anisotropy energy and forces the magnetization vectors to be parallel to each other over several grains. Under this condition, the effective anisotropy is averaged out and thus it leads to ultrasoft magnetic properties, i.e., low coercivity and very high permeability. Generally, the cause of superiority in these magnetic properties is mainly interpreted by structural developments in the bulk material during the nanocrystallization process. However, some reports suggested that the formation of crystallites occurred more easily in the surface than in within the bulk [6, 7]. In fact, there is evidence that crystallites exists at the surface even in the as-quenched state [8]. On heat-treatment, the process of crystallization initiates at the surface and then propagates towards the bulk. Hence, it is

*Corresponding author: Tel: +82-41-850-8276,
Fax: +82-41-850-8271, e-mail: heebok@kongju.ac.kr

worth mentioning that the phenomenon of structural changes involved during the amorphous to nanocrystalline transformation on heat-treatment should be simultaneously manifested in both the surface and in the bulk region [9].

Several attempts have been performed to improve the soft magnetic properties and the giant magneto-impedance (GMI) effect of FINEMET-type alloys either by altering the average distance between the nanograins with the help of suitable heat treatments or by tailoring the Curie temperature of the amorphous phase through modifying the composition of the precursor alloy [10-15]. More recently, in order to gain new rudimentary insights into the nature of the crystallization process, the microstructural evolution and into magnetic properties of ultrafine FINEMET-type magnetic materials. The simultaneous addition of Cr and Au elements in the FINEMET alloy system has been made.

The present work is an attempt to investigate the influence of structural and surface morphological changes taking place in the surface and bulk region in the crystallization process as well as the changes of magnetic properties such as magnetic permeability, coercivity, and GMI effect in $Fe_{73.5-x}Cr_xSi_{13.5}B_9Nb_3Au_1$ (x = 1, 2, 3, 4, 5) alloys after thermal treatments. The parallel evolution of the microstructure, the surface morphology, the soft magnetic properties, and the GMI effect are correlated.

2. Experiment

Amorphous ribbons with nominal composition $Fe_{73.5-x}Cr_xSi_{13.5}B_9Nb_3Au_1$ (x = 1, 2, 3, 4, 5) of about 8 mm in width and 20 μm in thickness were produced from ingots using the standard single copper wheel melt spinning technique. The $Fe_{73.5-x}Cr_xSi_{13.5}B_9Nb_3Au_1$ (x = 1, 2, 3, 4, 5) nanocrystalline materials consisting of ultrafine grains dispersed in an amorphous matrix were obtained by annealing their amorphous alloys at the temperature of 540°C for 30 min. The samples were heated to a specific temperature (540°C), and then kept temperature constant during 30 min, finally cooled to the room temperature. All steps were performed in vacuum to protect the samples from the oxidation.

The microstructure of the as-quenched amorphous ribbon and annealed ones was examined by X-ray diffraction (XRD Bruker D5005) with Cu-K_α radiation. Differential scanning calorimetry (DSC SDT 2960-TA Instruments) was used to examine the crystallization process of the as-quenched ribbons. The change in surface morphology of the samples was analyzed using atomic force microscopy (AFM). An AC Permeagraph (AMH-410A, Walker) was employed to measure the room temperature permeability and coercivity of toroidal samples using the induction method. We studied the GMI effect in the annealed samples. Magneto-impedance (MI) measurements were carried out along the ribbons axis under a dc longitudinal applied magnetic field. The samples with a length of about 15 mm were used for all MI measurements. A computer-controlled RF signal generator with its power amplifier was connected to the sample in series with a resistor for monitoring the driving ac current. The ac current and the voltage across the sample, for calculating the impedance, could be measured by using digital multimeters (DMM) with RF/V probes. The external dc field, applied by a solenoid, was swept through the entire cycle equally divided by 800 intervals from −300 Oe to 300 Oe. The frequency of the ac current was varied from 1 to 10 MHz, while its amplitude was varied from 10 to 30 mA. The schematic diagram of the MI experimental system can be found elsewhere [16].

The GMI ratio can be defined as $\Delta Z/Z(\%) = 100\% \times [Z(H) - Z(H_{max})]/Z(H_{max})$. where H_{max} is the maximum applied dc magnetic field. In present experiment H_{max} = 300 Oe.

3. Results and Discussion

3.1. XRD and DSC analysis

First, the microstructure of the as-quenched samples was examined using X-ray diffraction method. As can be seen in Fig. 1, the XRD patterns of as-quenched amorphous alloys exhibited only one broad peak around 2θ= 45°, which appears as a diffuse halo, indicating the

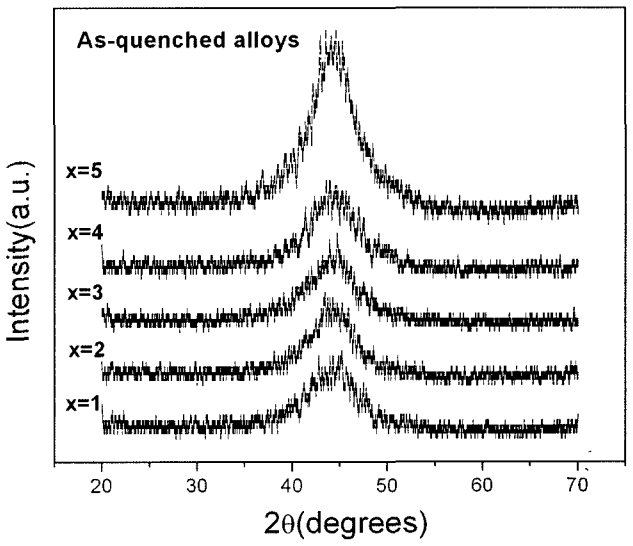

Fig. 1. The XRD patterns of as-quenched amorphous $Fe_{73.5-x}Cr_xSi_{13.5}B_9Nb_3Au_1$ (x = 1, 2, 3, 4, 5) alloys.

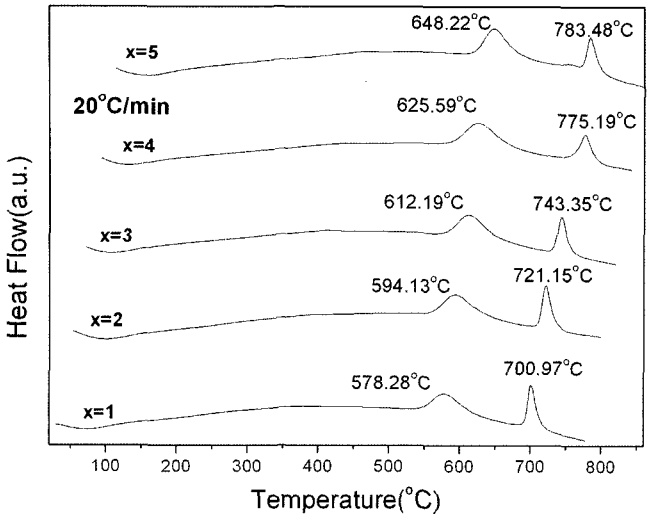

Fig. 2. The DSC curves of as-quenched $Fe_{73.5-x}Cr_xSi_{13.5}B_9Nb_3Au_1$ (x = 1, 2, 3, 4, 5) alloys (heating rate: 20°C/min).

amorphous state of the prepared samples.

A proper annealing regime for as-quenched amorphous alloys plays a decisive role in achieving the optimal soft magnetic properties [1]. We carried out DSC measurements in order to find out the most appropriate annealing temperature for as-quenched amorphous alloy composition. The DSC measurements give us very interesting information concerning the two main stages of crystallization. The DSC curves of the as-quenched amorphous alloys (x = 1~5) were performed at a heating rate 20°C/min. As can be seen clearly in Fig. 2, for all the samples, two stages of devitrification are observed. The first stage (578.28-648.22°C) depending on the Cr content corresponds to the nanocrystallization of the α-Fe(Si) soft magnetic phase and the second stage (700.97-783.48°C)

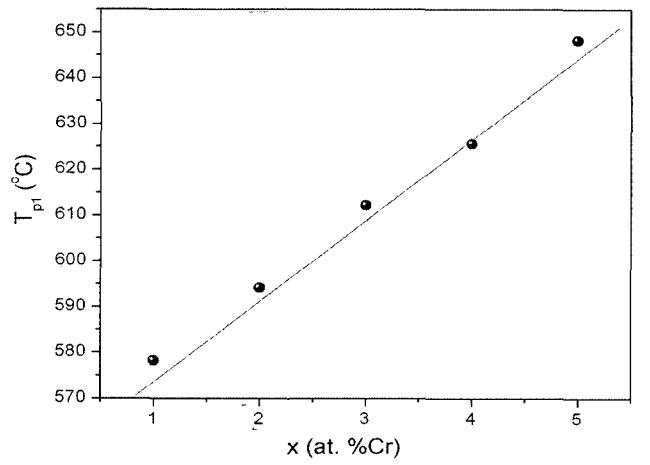

Fig. 3. Influence of Cr addition on the peak temperature of the first DSC exothermal. Heating rate: 20°C/min.

is related to the appearance of the boride-type phases (Fe_3B or Fe_2B) and recrystallization phenomena [17]. The influence of Cr addition on the temperature of the first crystallization peak (T_{p1}) was presented in Fig. 3. It is clearly that crystallization temperature of the α-Fe(Si) phase increases linearly with increasing Cr content in the studied range of composition. This indicates that the addition of Cr produces a slightly stabilization of the amorphous alloys against nanocrystallization.

Based on the DSC results, the as-quenched amorphous ribbon was annealed at T_a = 540°C for 30 min, in vacuum in order to obtain the nanocrystalline samples with the ultra-fine α-Fe(Si) phase. To confirm this feature, the microstructure of the nanocrystalline samples after annealing was examined by the XRD as shown in Fig. 4. It is clearly that, the α-Fe(Si) phase was detected in all the samples investigated. This indicated that, upon a proper heat treatment, the as-quenched amorphous state transformed in to the bcc structure nanograins with excellent soft magnetic properties. Furthermore, the particle size, d, of α-Fe(Si) grains can be determined from the breadth, B, of the X-ray diffraction peak (110), according to the Scherrer expression [18]:

$$d = \frac{0.9\lambda}{B\cos\theta_B} \quad (1)$$

Where λ is the X-ray wavelength (λ = 1.54056 Å), θ is the diffraction angle, and B is the full width at haft maximum (FWHM). Our calculations from the XRD patterns according to Eq. (1) revealed that, with increasing Cr content, the mean grain size of the samples decreased from ~6.2 nm (x = 1) to 5 nm (x = 5). These

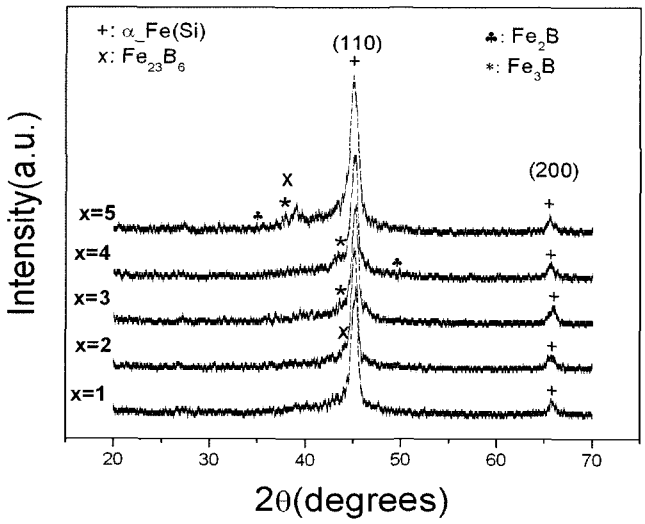

Fig. 4. The XRD patterns of the $Fe_{73.5-x}Cr_xSi_{13.5}B_9Nb_3Au_1$ (x = 1, 2, 3, 4, 5) alloys annealed at 540°C for 30 min.

results, together with the results obtained from DSC analyses, suggest that the Cr addition has a slowing down effect on the nanocrystallization kinetics leading to a smaller mean grain size of the α-Fe(Si) phase.

3.2. AFM analysis

The sufficient information of surface morphological features was examined using the AFM surface image experiments. A systematic study of AFM surface images has been performed for all investigated samples after annealing. In this work, we suppose that the role of Au in the studied samples is similar to that of Cu in FINEMET alloy. Besides, it is well-established that Cu element forms the cluster prior to the primary crystallization reaction of the α-Fe(Si) phase and Cu-enriched regions are observed at the grain boundaries [19]. As reported in Ref [8], some segregation of Cu atoms, which appear as bumps at the bottom of holes in amorphous matrix in the as-quenched FINEMET-type sample and act as seeds for crystallization was found. This is mainly attributed to insolubility of Cu atom in Fe leading its early partitioning on annealing. Figure 5 shows the AFM images of the surface morphology of the nanocrystalline samples (x = 2~5) annealed at 540°C for 30 min. As an example in Fig. 5a (for the x = 2 sample), surface image indicates the dispersion of cluster of protrusions of very high and uniform density. Such clustering in the amorphous matrix were those of Cu atoms as confirmed by Ayers *et al.* [19] using EXAFS technique. In our case, however, it is suggested that these clusters were of Au atoms dispersed in the amorphous matrix. These finely dispersed Au atoms acted as the nucleation centre for α-Fe(Si) crystallites. From the AFM surface images, the surface roughness (Rms) was determined and shown in Fig. 6. Furthermore, as observed in Figs. 5 and 6, with increasing Cr content, the large variation of density and size of protrusions along the ribbon plane was found (see Figs. 5a-5d), and simultaneously leads to the drastic change in the surface

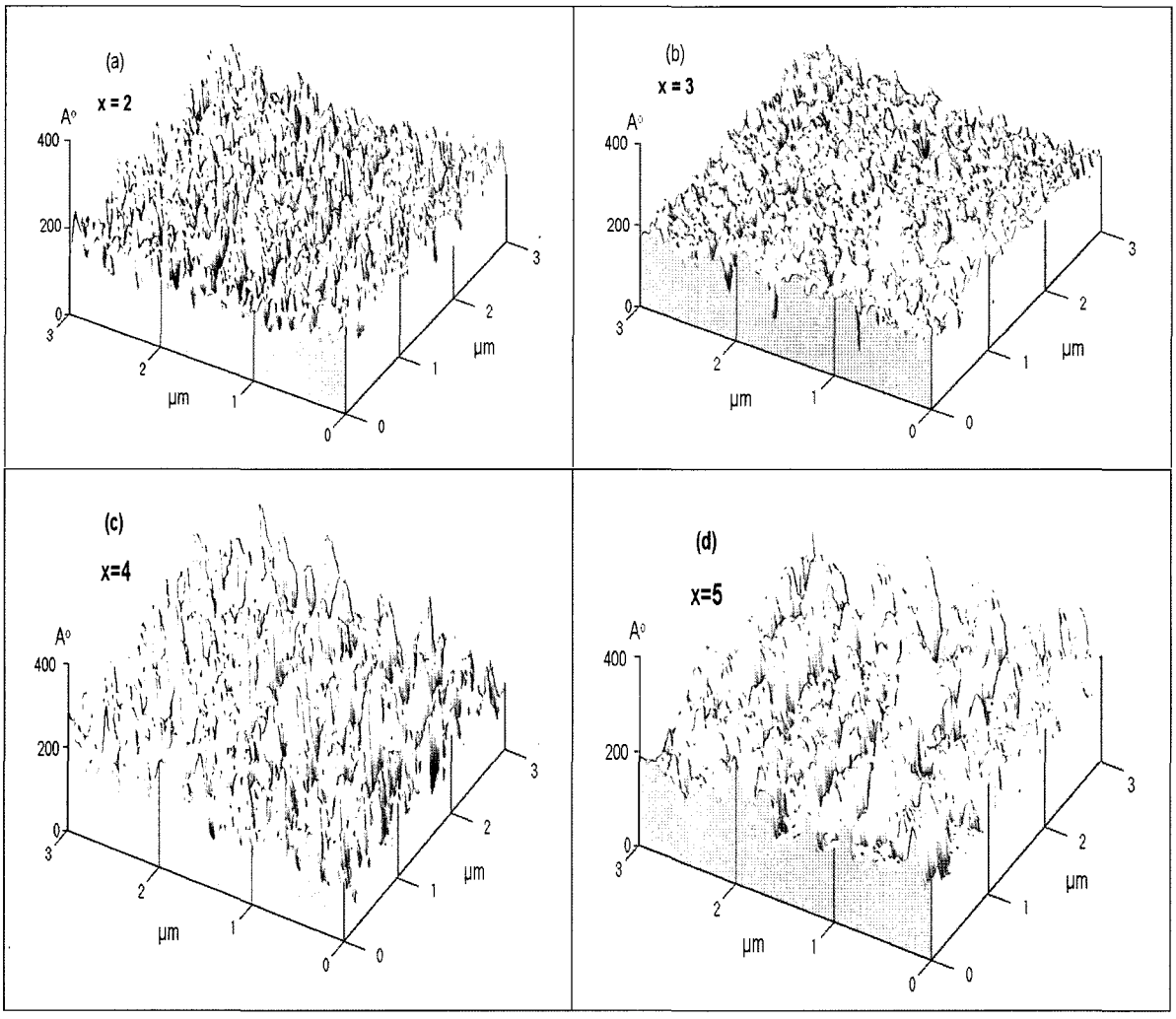

Fig. 5. AFM surface images of the nanocrystallized samples (x = 2, 3, 4, 5) annealed at T_a= 540°C for 30 min.

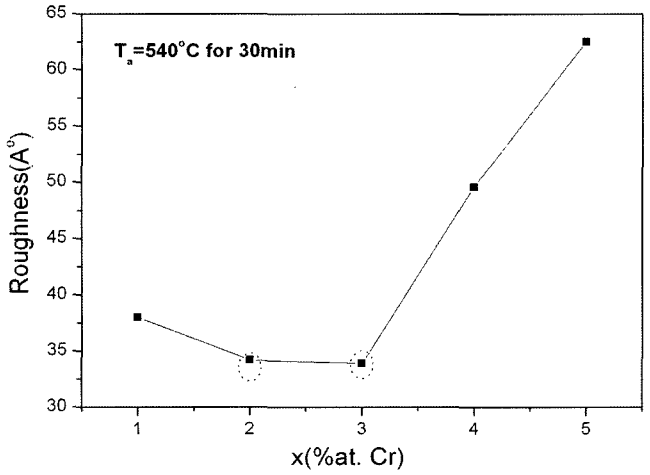

Fig. 6. Variations of Rms surface roughness calculated from AFM images for the samples (x = 1, 2, 3, 4, 5) annealed at 540°C for 30 min.

roughness (see Fig. 6). Among the samples investigated, the fine and uniform dispersion of protrusions along the sample plane which is related to the lowest value of surface roughness (~33.9 Å) was found in the x = 3 sample. These imply that the growth of Au clusters enhanced the nucleation reaction of the α-Fe(Si) phase, which improved the soft magnetic properties of this sample, i.e., the decrease of the coercivity, and the increase of the magnetic permeability (see Section 3.3). At both optimum Cr-doping level (x = 3) and annealing condition, the stage of nanocrystallite formation was found, where the bump in the form of protrusions tend to fill holes of amorphous matrix. The extension of singular protrusions along the ribbon surface became minimal indicating the crystallite growth of a primary phase of α-Fe(Si) nanoparticles [8]. The growth of these nanoparticles to an optimum size and volume fraction of the nanoparticles led to their soft magnetic properties. However, at higher Cr-doping levels (≥ 4), the broadening of protrusions and the drastic increase of roughness were observed. This is likely ascribed to the formation of additional multiples phases Fe-borides ($Fe_{23}B_6$, Fe_2B, and/or Fe_3B), as observed from XRD patterns (Fig. 4), further increased the relative height of the protrusions (see Figs. 5c and 5d). These sharp growth extensions increased the surface roughness of the samples (Fig. 6). These caused the deterioration of soft magnetic properties of the samples, i.e., an increase in coercivity (see Table 2) and a drop of the GMI effect in these samples, as found in Section 3.4.

Table 1. Magnetic characteristics of as-quenched amorphous ribbons $Cr_xFe_{73.5-x}Si_{13.5}B_9Nb_3Au_1$ (x = 1, 2, 3, 4, 5).

Sample	μ_i	μ_{max}	H_c (Oe)	M_s (emu/g)	B_{max} (kG)
x = 1	832	16,200	0.188	130	3.67
x = 2	980	12,000	0.070	126	3.47
x = 3	950	11,900	0.210	120	3.51
x = 4	850	15,000	0.067	116	3.47
x = 5	856	16,000	0.188	112	3.67

3.3. Magnetic softness analysis

It is pointed out that there is direct correlation between structure and its changes upon thermal treatments and parallel evolution of magnetic properties. The influence of partial substitution of Fe by Cr on the soft magnetic properties of $Fe_{73.5-x}Cr_xSi_{13.5}B_9Nb_3Au_1$ (x = 1, 2, 3, 4, 5) alloys was investigated. The magnetic hysteresis loops have been systematically studied for the samples annealed

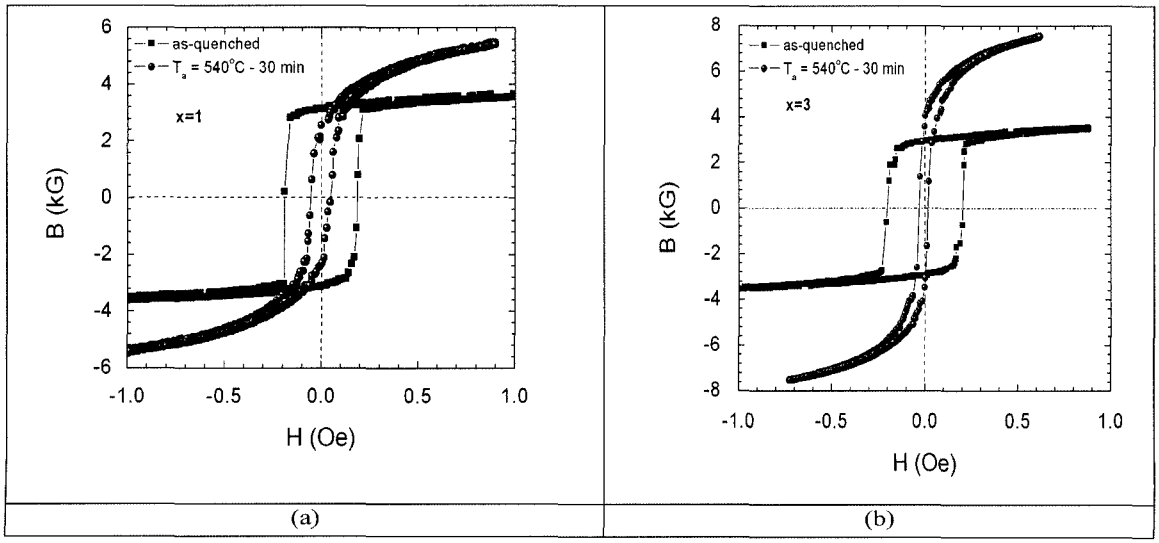

Fig. 7. Magnetic hysteresis loops of the samples, (a) x = 1 and (b) x = 3 (both as-quenched and annealed at 540°C for 30 min).

at 540°C for 30 min in vacuum. It was found that the addition of Cr causes a decrease in saturation magnetization which is entirely due to the dilution of Fe by Cr element. Additionally, the presence of Cr modified the magnetic characteristics of their precursor alloys (see Table 1). As examples, Figures 7a and 7b show the magnetic hysteresis loops of as-quenched amorphous and annealed alloy for the x = 1 and x = 3 samples. Accordingly, the magnetic characteristics of all studied samples were summarized in Tables 1 and 2. It is clearly that the hysteresis loops of the amorphous x = 1 and x = 3 samples showed the squared hysteresis loops which is due to the large value of coercivity. However, the hysteresis loops of the annealed samples have a normal form with improved soft magnetic properties. From Tables 1 and 2, it can be seen that the soft magnetic properties of the alloys are significantly improved upon suitable annealing. For instance, after annealing at 540°C for 30 min, the as-quenched amorphous state was transformed into ultrafine α-Fe(Si) nanograins with excellent soft magnetic properties caused by strongly magnetic exchange coupling between grains. As one can be seen clearly in Table 2, the 3% at Cr-containing sample exhibits the best soft magnetic properties characterized by the highest initial permeability (μ_i), maximum permeability (μ_{max}), and lowest coercivity (H_c). As a result, the largest GMI effect is observed in this sample (see Section 3.4). The improvement of soft magnetic properties in the x = 3 sample annealed at 540°C for 30 min is likely due to the formation of ultra-fine α-Fe(Si) phase and/or Fe_3Si nanoparticles at optimum conditions for both the grain size and crystalline content which reduced the magnetostriction constant of the material and hence magnetoelastic anisotropy. Furthermore, as mentioned in Section 3.2, the crystallization process of ultrafine α-Fe(Si) nanograins initiates at the surface region then propagates towards the bulk of the material.

It is worth mentioning that the formation of ultra-fine α-Fe(Si) nanograins (~6 nm) where magnetocrystalline anisotropies are averaged out, therefore nanocrystalline grains are strongly coupled though magnetic exchange interactions, thus leading to the ultrasoft magnetic properties. Meanwhile, with further increasing Cr content ($x \geq 4$), the formation of additional multiples phases ($Fe_{23}B_6$, Fe_2B and/or Fe_3B) which have highly magnetic anisotropy [1] was observed and also evidenced with the broadening together with the increase of the height of the protrusions from the AFM surface analysis. Therefore, it can be suggested that the strong magneto-anisotropic effect of Fe-boride phases together with the drastic variations in the surface profiles indicated by high roughness, which is supported to impede smooth movement of domain wall, deteriorated the soft magnetic properties of the samples (see Table 2).

Table 2. Magnetic characteristics of annealed ribbons $Cr_xFe_{73.5-x}Si_{13.5}B_9Nb_3Au_1$ (x = 1, 2, 3, 4, 5; T_a = 540°C for 30 min) and the maximum value of GMI ratio, $(\Delta Z/Z)_{max}$ (%), measured at 2 MHz.

Sample	μ_i	μ_{max}	H_c (Oe)	B_{max} (kG)	$(\Delta Z/Z)_{max}$ (%)
x = 1	11,800	28,000	0.044	5.47	84.72
x = 2	13,000	40,100	0.029	10.61	115.68
x = 3	23,000	50,500	0.028	7.54	157.95
x = 4	11,000	22,100	0.047	7.53	57.2
x = 5	12,200	19,000	0.051	8.84	41.52

3.4. GMI effect analysis

Recently, a very interesting phenomenon, so-called magnetoimpedance (MI) effect, has been observed in soft magnetic amorphous and nanocrystalline materials, which has attracted much interest because of its importance for applications in micromagnetic sensors and magnetic heads [20]. The MI phenomenon consists in a strong dependence of the electrical impedance, Z(f, H) = Z'(f, H) + j Z"(f, H) ($j = \sqrt{-1}$), of a ferromagnetic conductor on an external static magnetic field, H, when a high-frequency alternating current flows through it. The origin of the MI effect can be understood in a context of classical electrodynamics. In spite of difficulties in solving simultaneously the Maxwell equations and Landau-Lifshitz-Gilbert equation of motion for ferromagnetic conductors, it can be shown that in a uniform magnetic media this effect is explained on the basis of the impedance dependence on classic skin penetration depth, $\delta = (\rho/\pi f \mu_t)^{1/2}$, which is a function of frequency, f, of the ac current flowing across the conductor, the electrical resistivity, ρ, and the transverse magnetic permeability, μ_t, of the ferromagnetic sample. Therefore, these two parameters (ρ and μ_t) play an important role in the behavior of the MI effect. As mentioned, impedance Z depends on the transverse magnetic permeability, therefore, in the frame of outstanding magnetic softness the anisotropy features such as high-order anisotropy and non-uniform anisotropy distributions may play a key role in the total value of MI. As mentioned above, it is pointed out that the Cr-doping nanocrystalline materials with excellent soft magnetic properties are formed after proper annealing treatments. Consequently, Cr-doped nanocrystalline alloys are expected to have considerable magnetoimpedance effect due to their excellent soft magnetic properties: high permeability and low coercivity.

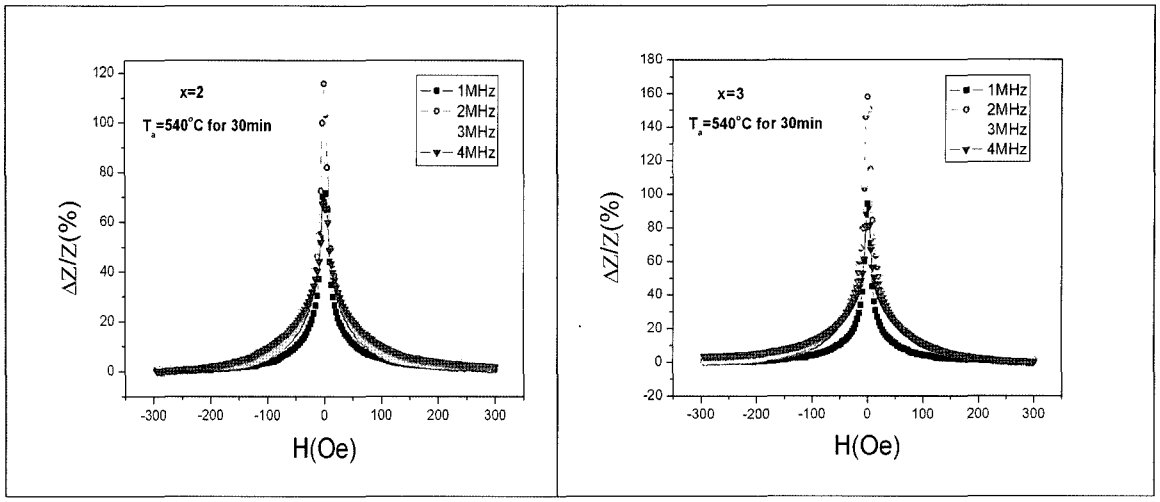

Fig. 8. The dc magnetic field dependence of ΔZ/Z for the nanocrystalline samples (a) x = 2 and (b) x = 3 at various frequencies up to f = 4 MHz.

Now, let us analyze some example data. The GMI profiles (ΔZ/Z) were measured as a function of the external dc magnetic field (H_{dc}) at various frequencies up to f = 4 MHz. These results obtained for the nanocrystallized samples (i.e., the amorphous alloys annealed at 540°C for 30 min) are given as the examples in Figs. 8a and 8b for the x = 2 and 3 samples, respectively. It can be seen that the maximum value of GMI was observed at near zero field (H_{dc} ~ 0) and the GMI profile had a single-peak feature. Among the samples studied (x = 1~5), the 3 at% Cr-containing sample exhibits the best GMI effect (see Fig. 8b) and the maximum GMI value reached the highest value of 160% at a measuring frequency of 2 MHz which is ideal for developing quick-response magnetic sensors. Accordingly, the higher GMI value observed at f = 2 MHz is likely due to the presence of its special domain structure as transverse domain patterns formed by a magneto-mechanical coupling between internal stress and magneto-striction which increased the transverse magnetic permeability of the sample and hence GMI value [21]. Based on obtained results, it is interesting to mention that, after proper thermal annealing (T_a = 540°C), the lowest surface roughness (see Section 3.2) together with excellent soft magnetic properties of the largest permeability and the lowest coercivity (see Section 3.3) were found in the 3 at% Cr-containing sample. These lead to the observed best GMI effect in this sample. Nevertheless, with higher Cr-doping levels (x ≥ 4), the reduction of GMI effect was observed and mainly ascribed to the deterioration of soft magnetic properties of the samples, i.e., an increase in coercivity (see Table 2). Concerning the decrease in the GMI effect with further Cr addition, another factor should be considered is that the resistivity of the sample with increasing Cr content. This may lead to a considerable decrease in the GMI effect for samples doping high Cr concentration [12].

The frequency dependence of the maximum GMI value (denoted as $[\Delta Z/Z]_{max}$ (%)) for all samples is shown in Fig. 9. Clearly, the GMI profiles first increased with increasing frequency up to f = 2 MHz and then decreased at higher frequencies. These findings can be interpreted by adapting the model of the skin effect for thin ribbons [22]. At frequencies below 1 MHz, the maximum value of GMI, $[\Delta Z/Z]_{max}$ (%), was relatively low due to the contribution of the induced magneto-inductive voltage to MI. When 1 MHz ≤ f ≤ 4 MHz, the skin effect is dominant, a higher $[\Delta Z/Z]_{max}$ (%) was found. Beyond f =

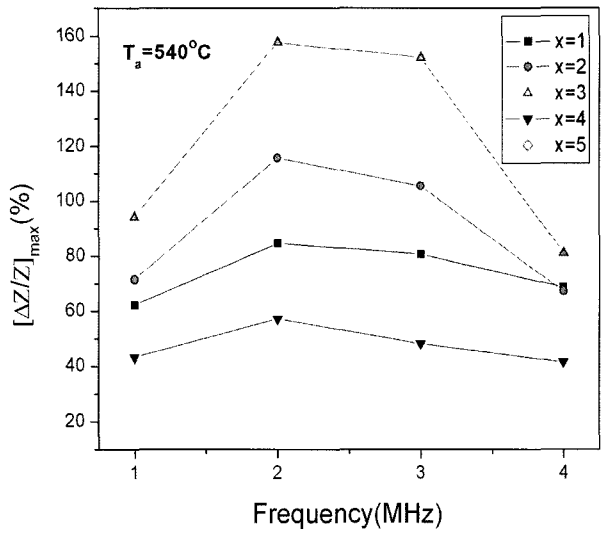

Fig. 9. The frequency dependence of $[\Delta Z/Z]_{max}$ for nanocrystalline $Fe_{73.5-x}Cr_xSi_{13.5}B_9Nb_3Au_1$ (x = 1, 2, 3, 4, 5) alloys.

4 MHz, the $[\Delta Z/Z]_{max}$ (%) decreases drastically with increasing frequency. It is believed that, in this frequency region ($f \geq 4$ MHz), the domain wall displacements were strongly damped owing to eddy currents thus contributing less to the transverse permeability, i.e., a small $[\Delta Z/Z]_{max}$ (%). In this context, it should be noted that the results from GMI analyses (Section 3.4) can be correlated to those from the magnetic softness (Section 3.3) and the AFM surface images (Section 3.2) as well as the microstructural changes (Section 3.1).

4. Conclusions

The influences of microstructural and surface morphological developments on the soft magnetic properties in conjunction with the GMI effect of $Fe_{73.5-x}Cr_xSi_{13.5}B_9Nb_3Au_1$ (x = 1, 2, 3, 4, 5) alloys have been thoroughly investigated and following results obtained:

a) The addition of Cr produces a slightly stabilization of the amorphous alloys against nanocrystallization and slightly decreases the mean grain size of the α-Fe(Si) phase.

b) AFM analysis reveals that the role of Au in the studied samples is similar to that of Cu in FINEMET alloy. The crystallization process of ultrafine α-Fe(Si) nanograins initiates at the surface region and then propagates towards the bulk of the material.

c) The large variation of surface morphology of density and size of protrusions along the ribbon plane was observed with various Cr content. Accordingly, the fine and uniform dispersion of protrusions which is related to the lowest value of surface roughness (~33.9 Å) was found in the x = 3 sample.

d) Ultrasoft magnetic properties of the nanocrystalline samples (x = 1~5) were significantly improved by properly annealing at T_a=540°C such as an increase of the magnetic permeability and the decrease of the coercivity.

e) The largest GMI effect was observed in the 3 at% Cr-doping sample among the studied samples, which is mainly related to the excellent properties of the lowest surface roughness, and largest magnetic softness was found in the sample. This sample can be used for high-performance GMI sensor applications.

Acknowledgments

The authors wish to acknowledge the Center for Materials Science, National University of Hanoi (Vietnam) kindly supplied the samples. This work was supported by Korean Science and Engineering Foundation through Research Center for Advanced Magnetic Materials at Chungnam National University.

References

[1] M. E. McHenry, M. A. Willard, and D. E. Laughlin, Prog. Mater. Sci. **44**, 291 (1999).
[2] Y. Yoshizawa, S. Oguma, and K. Yamauchi, J. Appl. Phys. **64**, 6044 (1988).
[3] P. Martin, M. Lopez, A. Hernando, Y. Iqbal, H. A. Davies, and M. R. J. Gibbs, J. Appl. Phys. **92**, 374 (2002).
[4] R. Alben, J. J. Becker, and M. C. Chi, J. Appl. Phys. **49**, 1653 (1978).
[5] G. Herzer, IEEE. Trans. Magn. **25**, 3327 (1989).
[6] U. Koster, Mater. Sci. Eng. **97**, 233 (1988).
[7] A. Gupta, and S. Habibi, Mater. Sci. Eng. A. **133**, 375 (1991).
[8] A. Slawska-Waniewska, A. Witck, and A. Reich, Mater. Sci. Eng. A. **133**, 363 (1991).
[9] A. K. Panda, M. Manimaran, A. Mitra, and S. Basu, Appl. Surf. Sci. **235**, 475 (2004).
[10] S. H. Lim, W. K. Pi, T. H. Noh, H. J. Kim, and I. K. Kang, J. Appl. Phys. **73**, 6591 (1993).
[11] C. G. Polo, P. Martin, L. Pascual, A. Hernando, and M. Vazquez, Phys. Rev B. **65**, 24433 (2001).
[12] M. H. Phan, H. X. Peng, S. C. Yu, N. D. Tho, and N. Chau, Acta. Mater (submitted).
[13] P. Agudo, and M. Vazquez, J. Appl. Phys. **97**, 23901 (2005).
[14] C. G. Polo, et al., J. Magn. Magn. Mater. **290**, 1517 (2005).
[15] N. Chau, N. Q. Hoa, and N. H. Luong, J. Magn. Magn. Mater. **290**, 1547 (2005).
[16] Heebok Lee, Y. K. Kim, K. J. Lee, and T. K. Kim, J. Magn. Magn. Mater. **215**, 310 (2000).
[17] M. H. Phan, H. X. Peng, M. R. Wiscom, S. C. Yu, and N. Chau, Composites, Part A (inpress).
[18] B. D. Cullity, Elements of X-ray diffraction, 2nd Ed, Addison-Wesley Publishing Company, Inc., Reading, MA (1978), pp. 102.
[19] J. D. Ayers, V. G. Harris, J. A. Sprague, and W. T. Elam, J. Appl. Phys. **64**, 974 (1994).
[20] V. M. Prida, P. Gorria, G. V. Kurlyandskaya, M. L. Sanchez, B. Hernando, and M. Tejedor, Nanotechnology. **14**, 231 (2003).
[21] M. H. Phan, H. X. Peng, M. R. Wiscom, S. C. Yu, and N. Chau, Phys. Status Solidi A **201**, 1558 (2004).
[22] L. V. Pannia, K. Mohri, T. Uchiyama, and M. Noda, IEEE Trans. Magn. **31**, 1249 (1995).